

Pan-cancer analysis of oncogene SFXN1 to identify its prognostic and immunological roles in lung adenocarcinoma

LIMING ZHANG¹, SHAOQIANG WANG² and LINA WANG³

¹Department of Thoracic Surgery, Weifang Second People's Hospital, Weifang, Shandong 261041, P.R. China;

²Department of Thoracic Surgery, Weifang People's Hospital, Weifang, Shandong 261000, P.R. China;

³Medical Research Center, Affiliated Hospital of Jining Medical University, Jining Medical University, Jining, Shandong 272029, P.R. China

Received September 25, 2024; Accepted January 14, 2025

DOI: 10.3892/or.2025.8883

Abstract. As cancer incidence and mortality rates continue to rise, the urgency for research in this field has increased globally. Sideroflexin 1 (SFXN1), a pivotal member of the SFXN protein family, serves a crucial role in transporting serine to mitochondria and participates in one-carbon metabolism, thereby influencing cell proliferation and differentiation. While SFXN1 is linked to lung cancer and glioma, its role in other malignancies remains largely unexplored. Utilizing The Cancer Genome Atlas, Human Protein Atlas, Gene Expression Profiling Interactive Analysis and University of Alabama at Birmingham Cancer Data Analysis Portal databases, the present study investigated the expression patterns, prognostic implications and association with immune cell infiltration of SFXN1. The present findings revealed that SFXN1 was differentially expressed across various tumor types, and exhibited significant associations with clinicopathological features and patient prognosis. Through immune infiltration analysis, a significant correlation between SFXN1 and T cells, B cells and immune checkpoint genes was established in numerous tumor types. Notably, loss-of-function experiments demonstrated that silencing of SFXN1 decreased cell proliferation, migration and invasion, while simultaneously increasing apoptosis in lung adenocarcinoma cells. Collectively, these findings suggested that SFXN1 expression could potentially serve as a biomarker for tumor diagnosis and prognosis, also emerging as a novel therapeutic target in cancer immunotherapy. The present study highlights the critical role of SFXN1 in cancer biology and paves the way for future translational efforts aimed at leveraging its potential in clinical oncology.

Introduction

Global statistics indicate that cancer has become the primary cause of death, posing a significant threat to human health (1). Despite advancements in cancer treatment modalities, including surgery, chemotherapy, targeted therapy and immunotherapy, which have notably improved patient survival rates, individuals with advanced lung cancer continue to face poor overall survival (OS) rates (2). Consequently, there is a need to explore more effective strategies for the prevention, early detection and treatment of cancer. Additionally, understanding the pathophysiological processes that initiate and drive cancer progression is crucial, offering both theoretical insights and practical applications.

The inner mitochondrial membrane of eukaryotic cells houses a class of transmembrane proteins referred to as sideroflexins (SFXNs), which were previously presumed to function solely as iron-utilizing metabolite transporters with limited known molecular roles (3,4). Serine, rich in one-carbon units, serves a pivotal role in supplying the one-carbon units essential for anabolic processes in dividing human cells (5,6). Mitochondrial serine metabolism predominantly fulfills this requirement, with cytosolic serine-driven one-carbon metabolism providing supplementary support when required (7). Among the SFXN family, SFXN1 has emerged as a key player in one-carbon metabolism and mitochondrial iron homeostasis, exerting effects on cellular proliferation, development and other vital biological processes (8-11). Emerging evidence suggests a robust association between SFXN1 and various malignancies, including lung cancer and glioma (12,13). Given that SFXN1 functions as an iron regulatory protein, its dysregulated expression may serve a role in the process of carcinogenesis (12). It has been hypothesized that SFXN1 expression on the mitochondrial membrane triggers the generation of reactive oxygen species (ROS) and iron accumulation, leading to ferroptosis in cancerous cells and potential organ damage (14). During ferroptosis, iron overload and lipid peroxidation act as central mediators, instigating oxidative damage to cellular membranes, a process critical to the execution of this non-apoptotic form of cell death (15).

The present study utilized publicly accessible databases to examine SFXN1 expression profiles in tumor tissues, investigating its prognostic significance in patients with

Correspondence to: Dr Lina Wang, Medical Research Center, Affiliated Hospital of Jining Medical University, Jining Medical University, 89 Guhuai Road, Jining, Shandong 272029, P.R. China
E-mail: wanglina_china@163.com

Key words: sideroflexin 1, pan-cancer, prognosis, immune infiltration, bioinformatics analysis

cancer. The present study further delved into SFXN1 mutation patterns and the landscape of immune infiltration. These comprehensive analyses were undertaken with the overarching goal of providing a refreshed theoretical foundation to elucidate the fundamental mechanisms governing tumorigenesis. Simultaneously, the present study aimed to pinpoint innovative diagnostic and prognostic biomarkers for malignancies, thereby contributing to the advancement of personalized cancer care and management.

Materials and methods

SFXN1 expression in human tissues and pan-cancer. The Human Protein Atlas (HPA; <https://www.proteinatlas.org/>) (16) was used to examine SFXN1 expression in various human tissues and organs at the mRNA and protein levels utilizing transcriptomics and proteomics methods. For statistical analysis and visualization of SFXN1 expression in cancer, RNA-sequencing (RNA-seq) data were obtained from the ALL (pan-cancer) project in The Cancer Genome Atlas (TCGA; <https://portal.gdc.cancer.gov/>) (17). The data were processed using the \log_2 function and the R ggplot2 package (version 4.3.1; 2023-06-16; The Comprehensive R Archive Network) was utilized. The Tumor Immune Estimation Resource (TIMER; <https://cistrome.shinyapps.io/timer/>) (18) was employed to validate SFXN1 expression in various cancer types compared with that in normal tissues. Gene Expression Omnibus (GEO) is a public repository maintained by the National Center for Biotechnology Information for high-throughput gene expression data, including microarray and RNA-Seq data (<https://www.ncbi.nlm.nih.gov/gds/>). The GSE22820 (19), GSE44861 (20), GSE75241 (21), GSE107591 (22), GSE84784 (23), GSE32863 (24), GSE16515 (25) and GSE27342 (26) datasets were used to verify SFXN1 expression.

Tissue microarrays (TMAs). Human pan-cancerous TMAs (ZL-MTU122) were provided by Shanghai Zhuoli Biotech Company Co., Ltd. Tissues were fixed in 10% neutral buffered formalin at room temperature for 24 h, embedded in optimal cutting temperature compound and stored at -80°C . Sections were cut at $4\text{-}\mu\text{m}$ thickness, incubated with 3% hydrogen peroxide (H_2O_2) in methanol for 10-15 min at room temperature, and then washed with 1X PBS to remove residual H_2O_2 , to block endogenous peroxidase activity. Sections were permeabilized with 0.3% Triton-X 100, and blocked with 1X TBS containing 0.3% Triton-X 100 and 5% goat serum (BL210A; Biosharp Life Sciences) at room temperature for 30 min. Sections were incubated with a primary antibody against SFXN1 (1:100; ab127751; Abcam) at 4°C overnight. The goat anti-rabbit HRP-conjugated antibody (ASR1038; Abcepta) was diluted at 1:200, and applied as the secondary antibody at room temperature for 60 min. Sections were then incubated with 3, 3'-diaminobenzidine solution for 5-10 min at room temperature until the desired color intensity was achieved. Sections were washed with 1X PBS to terminate the reaction. Detection was performed using a light microscope equipped with the VIS DIA VisioMorph system (Visiopamm[®]; Visiopharm A/S). The location of each tumor type is shown in Table SI. Pan-cancer SFXN1 protein levels were explored

using data from the Clinical Proteomic Tumor Analysis Consortium (<https://ualcan.path.uab.edu/analysis-prot.html>) from the University of Alabama at Birmingham Cancer Data Analysis Portal (UALCAN; <https://ualcan.path.uab.edu/cgi-bin/ualcan-res.pl>) (27,28).

Association between SFXN1 expression and tumor clinico-pathologic features and prognosis. RNA-seq data and clinical data (T stage, N stage and clinicopathological stage) were downloaded from TCGA, and normal samples and samples without clinical information were excluded. The stats package (version 4.2.1; 2022-06-23; The Comprehensive R Archive Network) was used to perform various statistical analyses, the car package (version 3.1.0; 2023-06-16; The Comprehensive R Archive Network) was used for processing and enhancing the statistical analyses of regression modeling and the related diagnostics, and the ggplot2 package (version 4.3.1; 2023-06-16; The Comprehensive R Archive Network) was used for visualization of the results, enhancing the interpretability and presentation of the findings. Kaplan-Meier plotter (<https://kmplot.com/>) (29) integrates chip data from GEO, TCGA and other databases to provide prognostic information for a variety of cancer types. The present study explored the association between SFXN1 expression and prognosis [OS and disease-free survival (DFS)] in breast invasive carcinoma (BRCA), esophageal carcinoma (ESCA), head and neck squamous cell carcinoma (HNSC), kidney renal clear cell carcinoma (KIRC), liver hepatocellular carcinoma (LIHC), lung adenocarcinoma (LUAD), thyroid carcinoma (THCA), uterine corpus endometrial carcinoma (UCEC) and testicular germ cell tumors (TGCT). The cut-off value selected for dichotomizing the gene expression levels is typically chosen based on the median expression level of the gene in the dataset, which was also selected in the present study. The Gene Expression Profiling Interactive Analysis 2 (GEPIA2; <http://gepia2.cancer-pku.cn/#index>) (30) database is a public database that can analyze RNA-seq expression data from a total of 9,736 tumor samples and 8,587 normal samples from TCGA and Genotype-Tissue Expression projects. GEPIA2.0 was used to determine the association between SFXN1 expression and OS and DFS in pan-cancer.

Receiver operating characteristic (ROC) curve analysis. The R program pROC (version 1.18.0) (<https://www.rdocumentation.org/packages/pROC/versions/1.18.0>) was used to analyze the RNA-seq data in TCGA to draw the ROC curve. ggplot2 was used for visualization.

SFXN1 mutation analysis. The Memorial Sloan Kettering Cancer Center has created cBioPortal (<http://www.cbioportal.org/>) (31), a comprehensive open and multifunctional data mining, integration and visualization platform built on TCGA. The present study investigated the alteration frequency, mutation type, mutated site details and copy number alterations of SFXN1 in pan-cancer using cBioPortal.

The tumor mutation burden (TMB) is defined as the total number of base mutations per million tumor cells. It is widely acknowledged that the TMB serves as an emerging biomarker for predicting the efficacy of cancer immunotherapies (32-35). A high TMB indicates a greater number of neoantigens,

thereby providing more opportunities for T cell recognition. Clinically, the TMB is associated with an improved response to immune checkpoint inhibitors (36). Microsatellite instability (MSI) is caused by abnormal DNA mismatch repair, resulting in gene replication errors and tumor development, which is associated with tumor prognosis (37). The correlation of SFXN1 with TMB and MSI was determined using Spearman analysis, while radar plots were created using the fmsb package (version 0.7.5; <https://minato.sip21c.org/msb/>).

DNA methylation analysis of SFXN1 in pan-cancer. DNA methylation is a common form of epigenetic modification. The methylation levels of the SFXN1 promoter were examined using UALCAN (<https://ualcan.path.uab.edu/cgi-bin/ualcan-res.pl>) (27,28).

Association between pan-cancer immune subtypes and SFXN1 expression. The TISIDB (<http://cis.hku.hk/TISIDB/index.php>) (24) database, comprising 4,176 records from 2,530 papers and 988 genes associated with antitumor immunity, is a database for tumor immunoassays. The statistical analysis of the association between immunological subtypes and SFXN1 expression was performed using TISIDB.

Association between SFXN1 and cancer immunity. The RNA-seq data and clinical information for 33 tumor types were obtained from TCGA. For reliable immune score evaluation, the immunedeconv package (version 2.0.3; <https://github.com/omnideconv/immunedeconv>), which integrates six of the latest algorithms, including MCPOUNTER, QUANTISEQ and EPIC, was used. These algorithms have been systematically benchmarked, and each algorithm has its own unique performance and advantages.

RNA-seq expression (level 3) profiles and associated clinical data of 33 tumor types were downloaded from TCGA. The expression levels of eight immune checkpoint transcripts (SIGLEC15, TIGIT, CD274, HAVCR2, PDCD1, CTLA4, LAG3 and PDCD1LG2) were analyzed.

Single-cell sequencing. CancerSEA (<http://biocc.hrbmu.edu.cn/CancerSEA/>) (38) is a multi-functional website designed to comprehensively explore 14 different functional states of cancer cells at the single-cell level. SFXN1 expression and functional states at the single-cell level were examined using CancerSEA. The t-distributed stochastic neighbor embedding maps were drawn using the CancerSEA website.

Screening of SFXN1-related genes in pan-cancer. The top 200 SFXN1-related genes (Table SII) in pan-cancer were obtained from TCGA using GEPIA2.0. The protein-protein interaction (PPI) network of the related genes was constructed using Search Tool for the Retrieval of Interacting Genes/Proteins (version 12.0; <https://cn.string-db.org>), and visualized using Cytoscape (version 3.9.1; <https://cytoscape.org/>) with the CytoHubba plugin to identify the most important modules.

Gene ontology (GO) and kyoto encyclopedia of genes and genomes (KEGG) enrichment analysis. The Database for Annotation, Visualization and Integrated Discovery (DAVID) website (<https://david.ncifcrf.gov/>) is a health information

database with systematic biological function annotation information for a large number of genes and proteins (39). The selected SFXN1-related genes were analyzed by GO and KEGG enrichment analysis using DAVID to explore the possible biological processes, cellular components, molecular functions and pathways involved. The Chiplot (<https://www.chiplot.online/#BioPlot>) website was used to visualize the enrichment analyses.

Gene set enrichment analysis (GSEA) of SFXN1 in LUAD. LUAD RNA-seq data and clinical information were downloaded from TCGA to extract the expression data of the differentially expressed molecules. The DESeq2 package (version 1.40.1; <https://bioconductor.org/packages/release/bioc/html/DESeq2.html>) was used to analyze the single gene differences (Table SIII). The dataset comes from the MSigDB Collections database (<https://www.gsea-msigdb.org/gsea/msigdb>). The clusterProfiler package (version 4.8.1; <https://www.bioconductor.org/packages/release/bioc/html/clusterProfiler.html>) was utilized for GSEA.

Collection of human LUAD specimens. A total of 35 pairs of LUAD and adjacent non-cancerous tissues were collected from patients (22 male and 13 female patients) undergoing lung surgery at the Affiliated Hospital of Jining Medical University (Jining, China) between November 2021 and November 2022. The patient age ranged between 50 and 75 years, with a median age of 55 years. Prior to surgery, none of the patients had a documented history of cancer, nor had they undergone chemotherapy, radiotherapy or targeted therapies. Patients with a Karnofsky Performance Status score (40) of 70 or higher, without significant comorbidities such as uncontrolled hypertension, severe cardiac disease or active infection, and without a history of autoimmune diseases or immunosuppressive therapy within the past 6 months were included in the study. Each patient signed an informed consent form. The Ethics Committee of the Affiliated Hospital of Jining Medical University (Jining, China) examined and approved the present study (approval no. 2021-11-C009).

RNA extraction and reverse transcription-quantitative PCR (RT-qPCR). TRIzol reagent (Invitrogen; Thermo Fisher Scientific, Inc.) was used to extract total cellular RNA of LUAD tissues and cells. A commercial cDNA synthesis kit (SuperScript First-Strand Synthesis System; Thermo Fisher Scientific, Inc.) was utilized to generate cDNAs by reverse transcription according to the manufacturer's instructions. The SYBR Green Assay Kit (Takara Bio, Inc.) was used to detect the presence of mRNA. Using the Biosystems ViiA7 Sequence Detection System (ViiATM 7 Real-Time PCR System; Thermo Fisher Scientific, Inc.), RT-qPCR was carried out at least three times. The qPCR thermocycling conditions were as follows: Initial denaturation at 95°C for 30 sec; followed by 40 cycles of denaturation at 95°C for 5 sec, annealing at 60°C for 30 sec and extension at 72°C for 30 sec. SFXN1 expression was normalized to GAPDH using the 2^{-ΔΔC_q} method (41). The primers were as follows: SFXN1 forward, 5'-AGGAATTGTTCTCC TGGTCT-3' and reverse, 5'-AGGAAACAGGGCACAACA CA-3'; and GAPDH forward, 5'-TCTTTTGCGTCGCCAGCC GAG-3' and reverse, 5'-TGACCAGGCGCCCAATACGAC-3'.

Western blot analysis. Protein was extracted from tissues and cells using RIPA cleavage buffer (Abcam). A BCA assay was used for protein determination and 20 μ g protein was loaded per lane on a 10% polyacrylamide gel with SDS and separated by electrophoresis. The protein in the gel was transferred to a PVDF membrane (Sigma-Aldrich; Merck KGaA). The membrane was blocked for 60 min with 5% BSA (cat. no. 9048-46-8; Beijing Solarbio Science & Technology Co., Ltd.) at room temperature, then incubated overnight at 4°C with specific primary antibodies, including anti-SFXN1 (1:3,000 dilution; ab127751; Abcam) and anti-GAPDH (1:3,000 dilution; ab9485; Abcam) antibodies. The antibodies were removed and the membrane was washed with TBS-0.1% Tween-20 three times. Subsequently, the membrane was incubated with secondary antibodies (anti-rabbit IgG, HRP-linked antibody; 1:5,000; cat. no. SA-00001-2; Proteintech Group, Inc.) at room temperature for 1 h. The protein bands were detected using the Clarity Western ECL substrate kit (Bio-Rad Laboratories, Inc.) and visualized using a Tanon 5200 imaging system (Tanon Science and Technology Co., Ltd.). The intensity of the protein bands was semi-quantified using ImageJ software (1.52a; National Institutes of Health) and the protein expression levels were normalized to the respective GAPDH bands.

Cell culture and transfection. Two lung cancer cell lines (A549 and Calu-1) were purchased from The Cell Bank of Type Culture Collection of The Chinese Academy of Sciences. All cells were cultured in RPMI 1640 (Thermo Fisher Scientific, Inc.) medium containing 10% FBS (Thermo Fisher Scientific, Inc.) with 100 U/ml penicillin and 100 mg/ml streptomycin (Thermo Fisher Scientific, Inc.), and incubated at 37°C with 5% CO₂ in an incubator. Small interfering RNA (siRNA/si-) targeting SFXN1 (si-SFXN1) and its corresponding negative control (si-NC) were synthesized by Shanghai GenePharma Co., Ltd. Lipofectamine 3000 (Invitrogen; Thermo Fisher Scientific, Inc.) was utilized for cell transfection. A549 and Calu-1 cells (3 \times 10⁵ cells/well) were cultured in 6-well plates and transfected with siRNA (5 nM) at 37°C. The transfection medium was replaced with fresh complete medium containing serum and antibiotics after 18 h. Cells were harvested 48 h post-transfection and the knock-down efficiency was verified by RT-qPCR and western blotting. Other experiments were also performed at this timepoint. The targeting sequences were as follows: si-NC sense, 5'-UUCUCC GAACGUGUCACGUTT-3' and antisense, 5'-ACGUGACAC GUUCGGAAGTAATT-3'; si-SFXN1-1 sense, 5'-GCUGCUAAU UGCAUUAUATT-3' and antisense, 5'-UAUUAUGCAU UAGCAGCTT-3'; and si-SFXN1-2 sense, 5'-GGGAACAGC UUACGUUUCUTT-3' and antisense, 5'-AGAAACGUAAGC UGUUCCCTT-3'.

Cell counting kit-8 (CCK-8) assay. In a 96-well plate, 2 \times 10³ cells (A549 and Calu-1) were seeded and cultured in triplicate wells. A total of 10 μ l CCK-8 solution (CK04-100T; Dojindo Laboratories, Inc.) was added and cells were incubated at 37°C for 1 h. The absorbance was analyzed at 450 nm with a standard microplate reader (BioTek; Agilent Technologies, Inc.).

Scratch wound healing assay. Six-well plates with a cell density of 5 \times 10⁵ A549 and Calu-1 cells per well were cultured without 10% FBS. Upon achieving a cell confluence of 90%, the cells were scratched with 10-ml pipette tips and washed with PBS.

Culture medium without FBS was added to continue the culture. The images were captured under a light microscope at 0 and 24 h, and analyzed using ImageJ software (1.52a).

Transwell assay. The upper Transwell chamber was precoated with 1:8 diluted Matrigel (BD Biosciences) at 37°C for 1 h. A total of 5 \times 10⁴ transfected A549 and Calu-1 cells in serum-free RPMI 1640 medium were seeded in the upper chamber of an 8- μ m Transwell system at room temperature, while 0.6 ml RPMI 1640 medium supplemented with 10% FBS was added to the lower chamber in a 24-well plate. After incubation at 37°C for 48 h, the migrated cells were fixed with 4% paraformaldehyde for 20 min at room temperature and stained with 0.1% crystal violet solution for 30 min at room temperature. For quantification, images from five random fields were captured and the cells were counted under a light microscope.

Detection of cell apoptosis by flow cytometry. A total of 3 \times 10⁵ cells/well were cultured in a six-well plate. After 48 h of siRNA transfection, the cells were harvested, rinsed with PBS and re-suspended in 1X binding buffer. The cells were dual-stained with APC-Annexin V and 7-AAD (C1062L; Beyotime Institute of Biotechnology) at room temperature for 20 min and immediately analyzed by flow cytometry using the Beckman Coulter CytoFLEX instrument (Beckman Coulter, Inc.) to assess apoptosis. Data were acquired and analyzed using the Beckman Coulter CytExpert software (version 2.4; Beckman Coulter, Inc.).

Statistical analysis. To ensure accuracy, all experiments were independently repeated three times. All statistical analyses were performed using SPSS 23.0 software (IBM Corp.). The data are presented as the mean \pm SD. The expression differences between paired cancer and para-cancerous tissues were compared using a paired two-tailed t-test. For multiple groups, one-way ANOVA was used. Following a significant ANOVA result, the Tukey post hoc test was applied to pinpoint specific differences among the groups. The Wilcoxon rank sum test was used to determine the association between SFXN1 expression and the clinicopathological variables (pathologic T stage, pathologic N stage and pathologic stage) of the samples. The survival curve was plotted using the Kaplan-Meier method and groups were compared using the log-rank test. Spearman's rank correlation was used to quantitatively assess the relationship between SFXN1 expression levels and the infiltration of distinct immune cell populations. The relationship between SFXN1 expression and TMB and MSI was explored by Spearman's rank correlation analysis. The relationship between SFXN1 expression and tumor functional states was analyzed using Pearson's correlation coefficient. The positive correlation between SFXN1 and the top 20 genes across pan-cancer was assessed using Spearman's rank correlation analysis. $P < 0.05$ was considered to indicate a statistically significant difference.

Results

SFXN1 gene expression in human tissues and pan-cancer. To elucidate the role of SFXN1, the initial step was to examine its expression across different tissues. Through an extensive search of the HPA database, it was identified that SFXN1

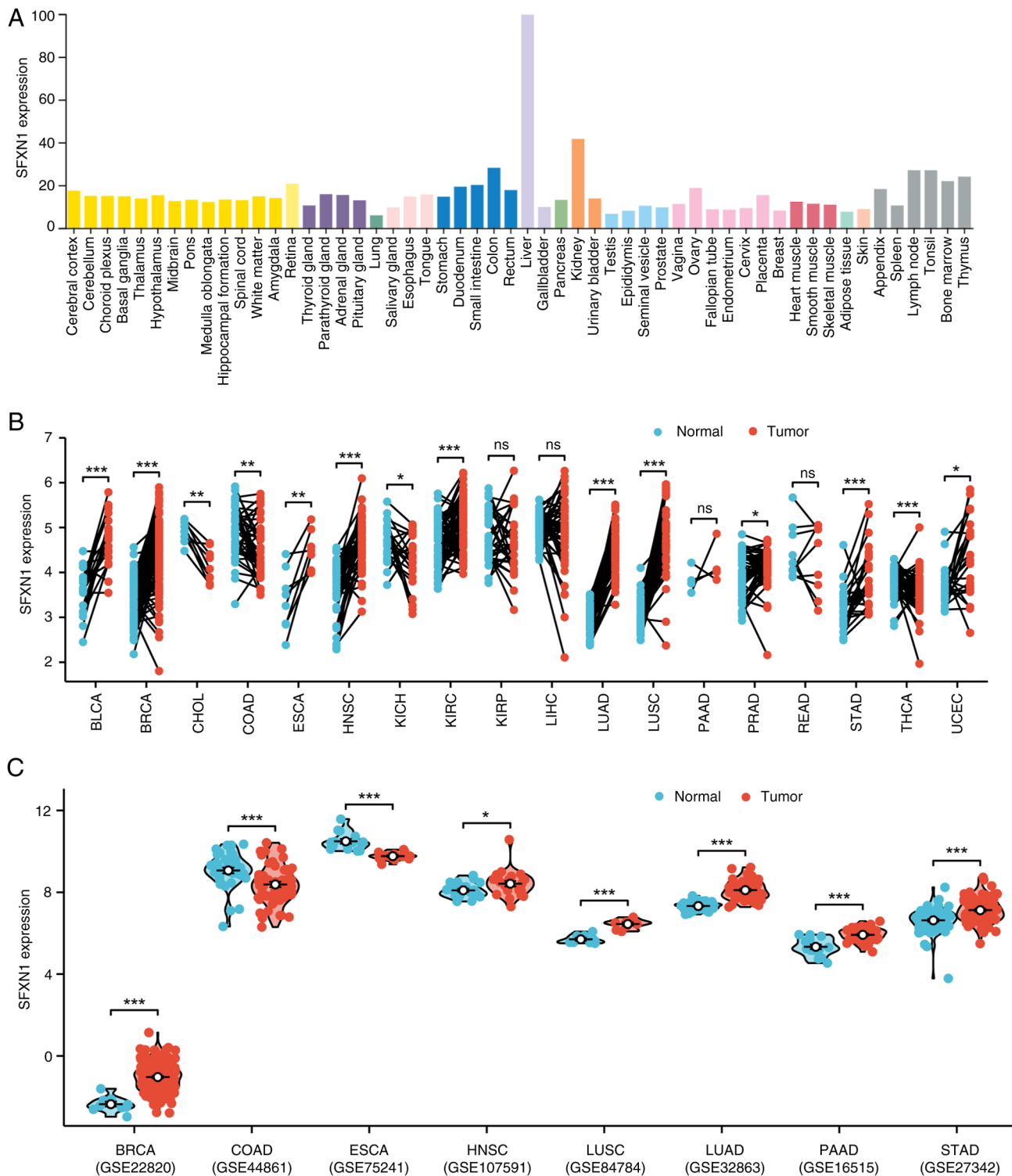


Figure 1. SFXN1 mRNA expression in human tissues based on (A) the Human Protein Atlas, (B) pan-cancer data from The Cancer Genome Atlas and (C) Gene Expression Omnibus datasets. * $P < 0.05$, ** $P < 0.01$ and *** $P < 0.001$. ns, not significant; SFXN1, sideroflexin 1.

expression was particularly high in the liver and kidney (Fig. 1A). Subsequently, SFXN1 expression in tumor tissues was investigated using data from TCGA and TIMER. Analysis of paired samples in TCGA revealed significantly elevated mRNA levels of SFXN1 in bladder urothelial carcinoma (BLCA; $P < 0.001$), BRCA ($P < 0.001$), ESCA ($P < 0.01$), HNSC ($P < 0.001$), KIRC ($P < 0.001$), LUAD ($P < 0.001$), lung squamous cell carcinoma (LUSC; $P < 0.001$), stomach adenocarcinoma

(STAD; $P < 0.001$) and UCEC ($P < 0.05$), and low expression in cholangiocarcinoma (CHOL; $P < 0.01$), colon adenocarcinoma (COAD; $P < 0.01$), kidney chromophobe (KICH; $P < 0.05$), prostate adenocarcinoma (PRAD; $P < 0.05$) and THCA ($P < 0.001$) (Fig. 1B). Furthermore, the pan-cancer non-paired data from TCGA indicated that SFXN1 expression was high in BLCA, BRCA, cervical squamous cell carcinoma and endocervical adenocarcinoma (CESC), ESCA, HNSC, KIRC, LUAD,

LUSC, STAD, and UCEC, and low in CHOL, COAD, KICH, kidney renal papillary cell carcinoma (KIRP), LIHC and THCA (Fig. S1A). Consistently, the findings from the TIMER database demonstrated elevated SFXN1 levels in BLCA, BRCA, CESC, ESCA, HNSC, LUAD, LUSC, STAD and UCEC, and decreased SFXN1 levels in CHOL, COAD, KICH, KIRP, LIHC and THCA (Fig. S1B). Furthermore, SFXN1 expression patterns were examined by incorporating validation from the GEO datasets GSE22820 (BRCA), GSE44861 (COAD), GSE75241 (ESCA), GSE107591 (HNSC), GSE84784 (LUSC), GSE32863 (LUAD), GSE16515 (PAAD) and GSE27342 (STAD) (Fig. 1C). Notably, SFXN1 expression was lower in ESCA and higher in PAAD tumor tissues, contrary to TCGA results.

SFXN1 protein expression in 20 types of cancer. TMAs were used to investigate the protein levels of SFXN1 in tumor tissues (Fig. 2A). The findings revealed that SFXN1 protein expression was elevated in BRCA, LIHC, LUAD, non-Hodgkin lymphoma, rectum adenocarcinoma (READ), small cell lung cancer and skin cutaneous melanoma (SKCM) compared with para-cancerous tissues (Fig. 2B-H), while it was lower in STAD (Fig. 2I). Furthermore, pan-cancer protein expression analysis indicated that there was a significant increase in SFXN1 protein expression in BRCA, COAD, UCEC, lung cancer, pancreatic cancer (PAAD) and HNSC, whereas a decrease was observed in KIRC, glioblastoma multiforme (GBM) and LIHC (Fig. 2J).

Association between SFXN1 expression and clinical features in cancer. The present study examined the association between SFXN1 expression and various pathological characteristics. SFXN1 mRNA expression was observed to be elevated in the advanced T stages of CESC, KIRP and PRAD, while it was decreased in the T3/T4 stages of KIRC and SKCM (Fig. 3A-E). In CESC and COAD, the mRNA levels of SFXN1 were found to be reduced in patients in the N1/2 stage compared with in those in the N0 stage (Fig. 3F and G). Conversely, in KICH, LUAD and LUSC, SFXN1 expression was increased in the N1/2/3 stages (Fig. 3H-J). Furthermore, SFXN1 expression was noted to be lower in stage III/IV of COAD and KIRC but was higher in stage III/IV in patients with KIRP, LUAD and UCEC (Fig. 3K-O).

Prognostic evaluation of SFXN1 in pan-cancer. The GEPIA2.0 database was employed to evaluate the impact of SFXN1 expression on pan-cancer prognosis, encompassing both OS and DFS. Elevated SFXN1 expression in adrenocortical carcinoma (ACC; $P=0.024$), LUAD ($P=0.042$), mesothelioma (MESO; $P=0.0046$) and acute myeloid leukemia (LAML; $P=0.00062$) was associated with adverse OS; however, elevated SFXN1 expression in KIRC was associated with good prognosis ($P=5.5 \times 10^{-6}$) (Figs. 4A and S2A-C). DFS analysis showed that high SFXN1 expression was associated with poor prognosis in patients with MESO ($P=0.041$) and sarcoma (SARC; $P=0.048$), and good prognosis in patients with KIRC ($P=0.00043$) (Fig. 4B).

The Kaplan-Meier plotter was used to validate the relationship between SFXN1 expression and tumor prognosis. The present findings demonstrated that high SFXN1 expression

was associated with poor OS in BRCA ($P=0.0043$), ESCA ($P=0.031$), HNSC ($P=0.013$), LUAD ($P=0.00041$), THCA ($P=0.0085$) and UCEC ($P=0.031$), and with favorable OS in KIRC ($P=6.9 \times 10^{-5}$) and LIHC ($P=0.042$) (Fig. S2D-K). Analysis of the recurrence-free survival (RFS) revealed that patients with higher SFXN1 expression had a shorter RFS in KIRC ($P=0.043$), LUAD ($P=0.0084$), TGCT ($P=0.025$) and THCA ($P=0.0068$) (Fig. S2L-O).

Diagnostic value of SFXN1 in pan-cancer. The present study subsequently investigated the potential of SFXN1 to serve as a diagnostic marker in pan-cancer using ROC curves. The area under the curve (AUC) indicated that SFXN1 possessed high diagnostic value in BLCA (AUC, 0.834), BRCA (AUC, 0.865), CESC (AUC, 0.948), CHOL (AUC, 0.898), ESCA (AUC, 0.906), HNSC (AUC, 0.867), LUAD (AUC, 0.980), LUSC (AUC, 0.986) and STAD (AUC, 0.900) (Fig. 4C-K).

Association between SFXN1 and pan-cancer immunity. The MCPOUNTER, QUANTISEQ and EPIC algorithms were used to assess the association between SFXN1 expression and immune cell infiltration. Based on the MCPOUNTER findings, SFXN1 expression was positively associated with CD8⁺ T cell infiltration in CESC, COAD, HNSC, PRAD, thymoma (THYM) and uveal melanoma (UVM), but negatively associated with CD8⁺ T cell infiltration in ACC, GBM, brain lower grade glioma (LGG) and TGCT. SFXN1 expression was positively associated with T cell infiltration only in THYM, but negatively associated with T cell infiltration in BLCA, BRCA, CESC, ESCA, GBM, HNSC, KIRC, LGG, LIHC, LUAD, LUSC, pheochromocytoma and paraganglioma (PCPG), READ, SKCM, STAD, TGCT and THCA. SFXN1 expression exhibited positive correlation with neutrophil infiltration in ACC, BLCA, BRCA, CESC, COAD, lymphoid neoplasm diffuse large B-cell lymphoma (DLBC), ESCA, HNSC, KICH, KIRC, KIRP, LAML, LIHC, LUSC, ovarian serous cystadenocarcinoma (OV), PAAD, PCPG, PRAD, SARC, SKCM, STAD, TGCT, THCA, UCEC, uterine carcinosarcoma (UCS) and UVM. As for natural killer (NK) cell infiltration, SFXN1 expression exhibited a negative association with this in GBM, LGG, MESO and THYM, and a positive association with this in COAD, HNSC, LAML, PAAD, PRAD, READ and UVM. SFXN1 expression exhibited a negative correlation with myeloid dendritic cell infiltration in BRCA, GBM, LGG, LUSC, OV, STAD, TGCT and UCEC, but a positive correlation with myeloid dendritic cell infiltration in KIRC, PRAD, THCA, THYM and UVM. SFXN1 expression was negatively associated with monocyte and macrophage/monocyte infiltration in ACC, GBM, LIHC, SARC, TGCT and THYM, and positively associated with monocyte and macrophage/monocyte infiltration in BLCA, CESC, COAD, HNSC, KIRC, PRAD, SKCM, STAD and UVM. As for endothelial cell infiltration, SFXN1 expression was negatively associated with this in BRCA, ESCA, LUAD, LUSC and STAD, but positively associated with this in CESC, DLBC, HNSC, KIRC, KIRP, LAML, LIHC, OV, PAAD, PRAD, SKCM, TGCT, THCA and UVM. SFXN1 expression exhibited a significant negative correlation with B cell infiltration in BRCA, ESCA, GBM, KIRC, LGG, LUAD, LUSC, OV, TGCT and UCEC (Fig. 5A).

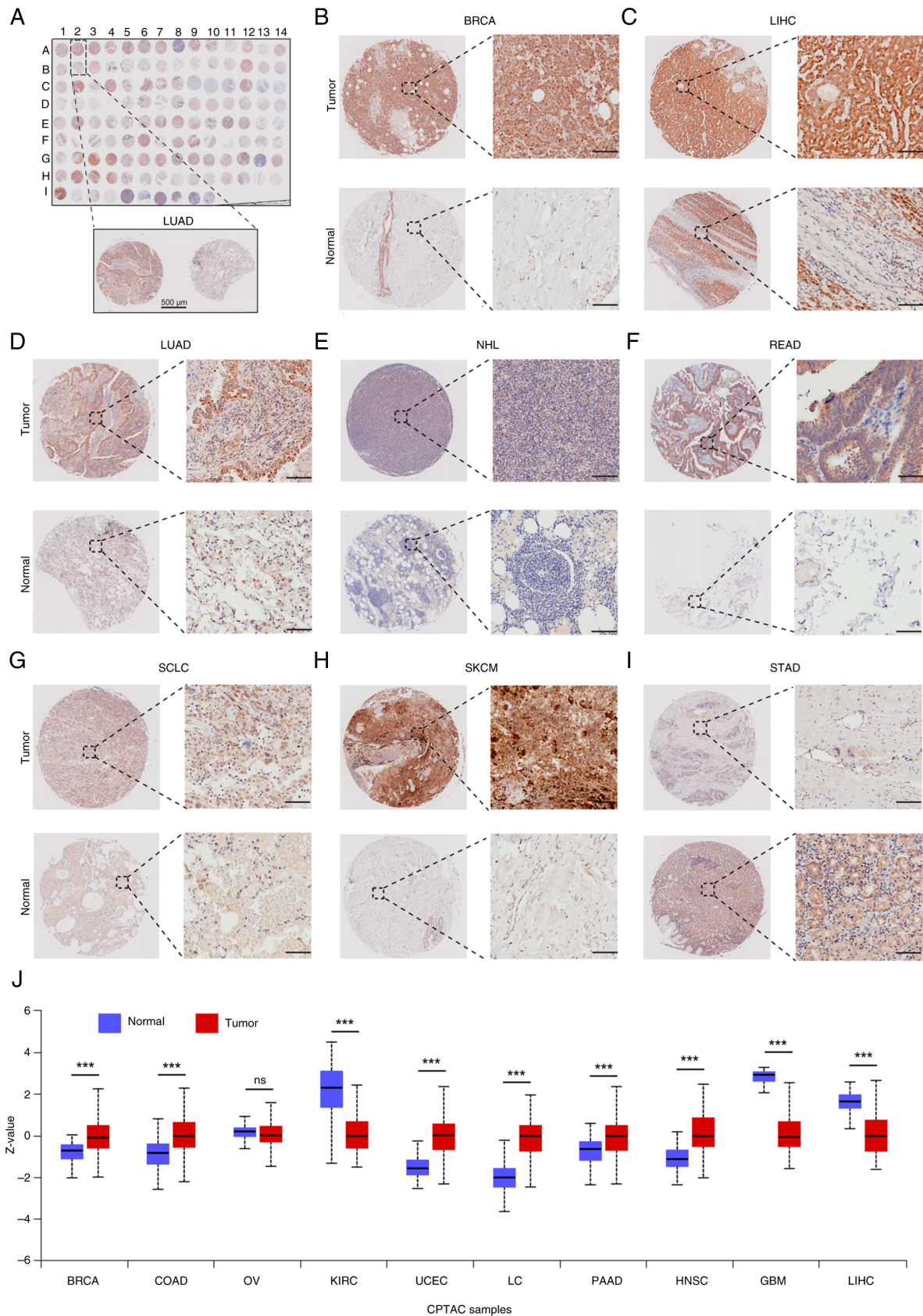


Figure 2. SFXN1 protein expression in 20 types of cancer. (A) Tissue microarray (TMA) of SFXN1 protein expression in 20 types of cancer. Scale bar, 500 μ m. SFXN1 protein expression in (B) BRCA, (C) LIHC, (D) LUAD, (E) NHL, (F) READ, (G) SCLC, (H) SKCM and (I) STAD. Scale bar, 100 μ m. (J) Pan-cancer SFXN1 protein levels based on the University of Alabama at Birmingham Cancer Data Analysis Portal database. ***P<0.001. BRCA, breast invasive carcinoma; CPTAC, Clinical Proteomic Tumor Analysis Consortium; LIHC, liver hepatocellular carcinoma; LUAD, lung adenocarcinoma; NHL, non-Hodgkin lymphoma; ns, not significant; PAAD, pancreatic adenocarcinoma; RCC, renal cell carcinoma; READ, rectum adenocarcinoma; SCLC, small cell lung cancer; SFXN1, sideroflexin 1; SKCM, skin cutaneous melanoma; STAD, stomach adenocarcinoma; COAD, colon adenocarcinoma; OV, ovarian serous cystadenocarcinoma; KIRC, kidney renal clear cell carcinoma; UCEC, uterine corpus endometrial carcinoma; LC, lung cancer; PAAD, pancreatic adenocarcinoma; HNSC, head and Neck squamous cell carcinoma; GBM, glioblastoma multiforme.

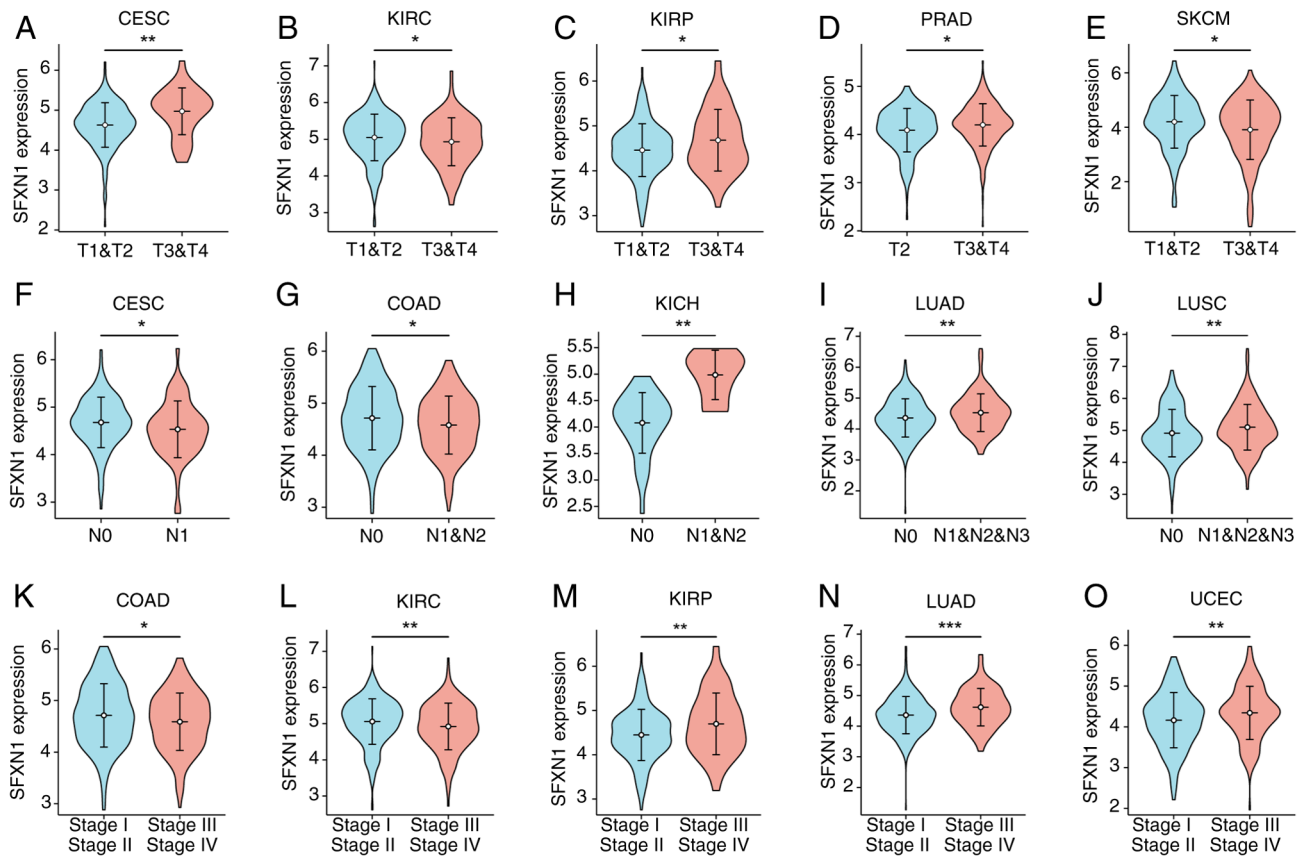


Figure 3. Relationship between SFXN1 mRNA expression and clinical features in different cancer types. Relationship between SFXN1 mRNA expression and T stage in (A) CESC, (B) KIRC, (C) KIRP, (D) PRAD and (E) SKCM. Relationship between SFXN1 expression and N stage in (F) CESC, (G) COAD, (H) KICH, (I) LUAD and (J) LUSC. Relationship between SFXN1 expression and pathological stage in (K) COAD, (L) KIRC, (M) KIRP, (N) LUAD and (O) UCEC. * $P < 0.05$, ** $P < 0.01$ and *** $P < 0.001$. CESC, cervical squamous cell carcinoma and endocervical adenocarcinoma; COAD, colon adenocarcinoma; KICH, kidney chromophobe; KIRC, kidney renal clear cell carcinoma; KIRP, kidney renal papillary cell carcinoma; LUAD, lung adenocarcinoma; LUSC, lung squamous cell carcinoma; PRAD, prostate adenocarcinoma; SFXN1, sideroflexin 1; SKCM, skin cutaneous melanoma; UCEC, uterine corpus endometrial carcinoma.

QUANTISEQ findings showed that SFXN1 expression was negatively associated with regulatory T cells in ESCA, KIRC, LUAD and LUSC, and positively associated with regulatory T cells in COAD, HNSC, LAML, LGG, PAAD, PCPG, PRAD and SKCM. As for CD8⁺ T cell infiltration, SFXN1 expression was negatively associated with this in ACC, GBM, LGG and UCEC, but positively associated with this in COAD, DLBC, HNSC, LAML, PRAD, THYM and UVM. SFXN1 expression exhibited a negative association with CD4⁺ T cells in PRAD, STAD and UVM, and a positive association with CD4⁺ T cells in BRCA, COAD, GBM, HNSC, KIRC, LAML, LGG, LUSC and TGCT. SFXN1 expression was negatively associated with neutrophil infiltration in BRCA and LUSC, but positively associated with neutrophil infiltration in COAD, HNSC, KICH, KIRC, KIRP, LIHC, PAAD, PRAD, STAD, TGCT and THCA. SFXN1 expression exhibited a significant negative correlation with NK cell infiltration in BLCA, COAD, KIRP and LUAD, and a positive correlation with NK cell infiltration in GBM, HNSC, KIRC, LGG, LIHC, PAAD, PGPC, STAD, TGCT and UVM. SFXN1 expression exhibited an obvious negative association with myeloid dendritic cell infiltration in KIRC, LIHC and TGCT, whereas it exhibited a positive association with myeloid dendritic cell infiltration in ACC, KIRP, LUAD, PAAD, PCPG, PRAD, READ, SARC, SKCM

and THCA. SFXN1 expression was negatively associated with monocyte infiltration in KIRC, KIRP, PCPG, PRAD, THCA and THYM, but positively associated with monocyte infiltration in GBM and TGCT. As for infiltration of M2 macrophages, SFXN1 expression exhibited a negative association with this in ACC, COAD, GBM, KIRP, LGG, LUAD, READ, SARC, STAD, TGCT and THYM, but a positive association with this in BRCA, CHOL, HNSC, PAAD, PRAD and UVM. SFXN1 expression exhibited an obvious negative association with M1 macrophage infiltration in GBM, LGG, LIHC, LUSC, PCPG, SARC, TGCT, THCA and THYM, while exhibiting a positive association with M1 macrophage infiltration in CESC, COAD, HNSC, PAAD, PRAD, READ, STAD and UVM. SFXN1 expression exhibited a significant negative association with B cell infiltration in ESCA, KIRC, LUAD, STAD and TGCT, but a positive association with B cell infiltration in LGG, PRAD and UVM (Fig. 5B).

According to the EPIC results, SFXN1 expression was negatively associated with CD8⁺ T cell infiltration in ESCA, HNSC, LUAD, STAD and TGCT, but positively associated with CD8⁺ T cell infiltration in BRCA, COAD, KICH, KIRC, KIRP, LGG, PCPG, PRAD, THYM and UVM. SFXN1 expression was negatively associated with CD4⁺ T cell infiltration in MESO and TGCT, and positively associated with CD4⁺ T cell

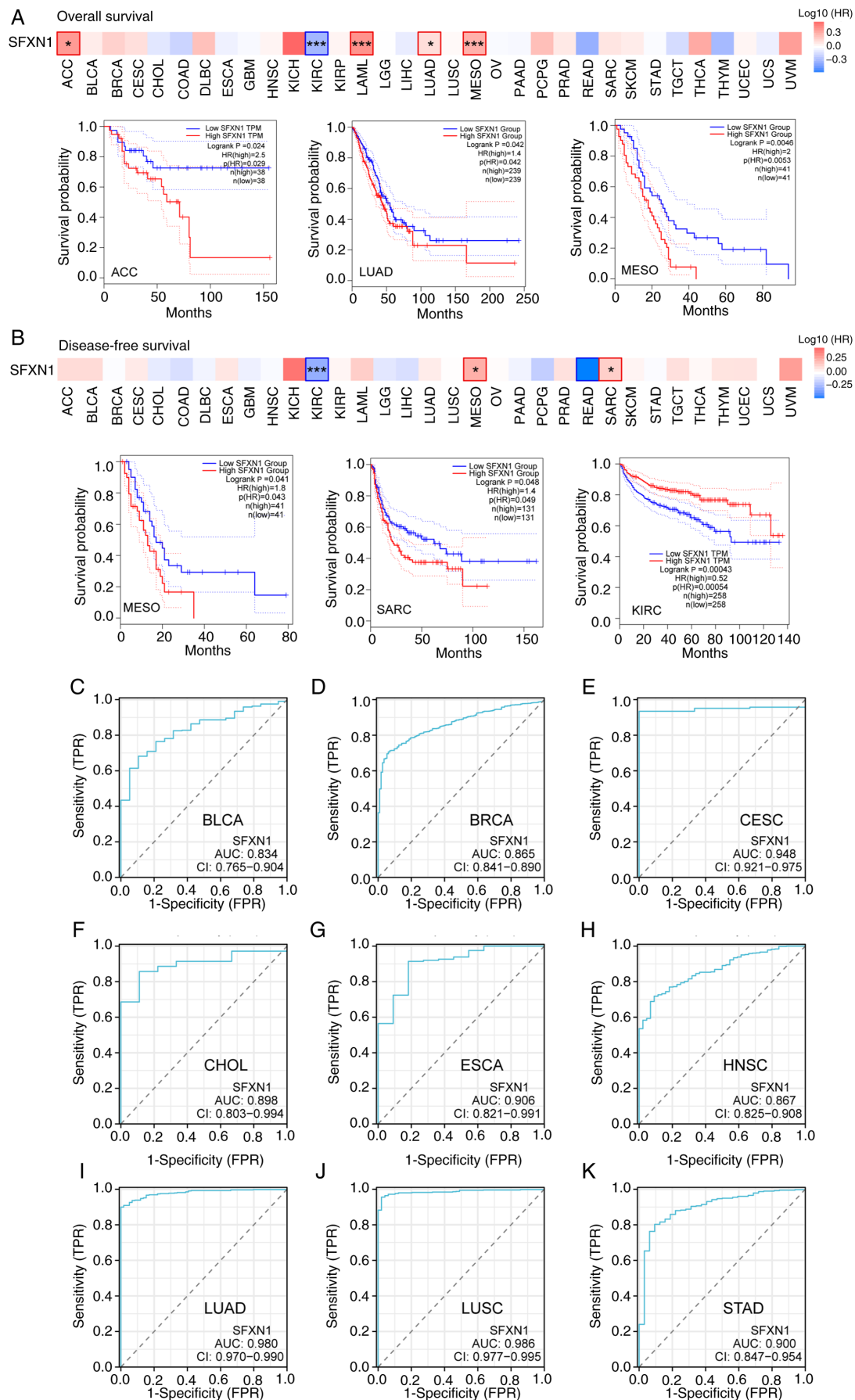


Figure 4. Prognostic and diagnostic value of SFXN1 in pan-cancer. Association between SFXN1 expression and (A) overall survival and (B) disease-free survival in pan-cancer. Receiver operating characteristic curves of SFXN1 in (C) BLCA, (D) BRCA, (E) CESC, (F) CHOL, (G) ESCA, (H) HNSC, (I) LUAD, (J) LUSC and (K) STAD. *P<0.05 and ***P<0.001. AUC, area under the curve; FPR, false positive rate; HR, hazard ratio; SFXN1, sideroflexin 1; TPM, transcripts per million; TPR, true positive rate.

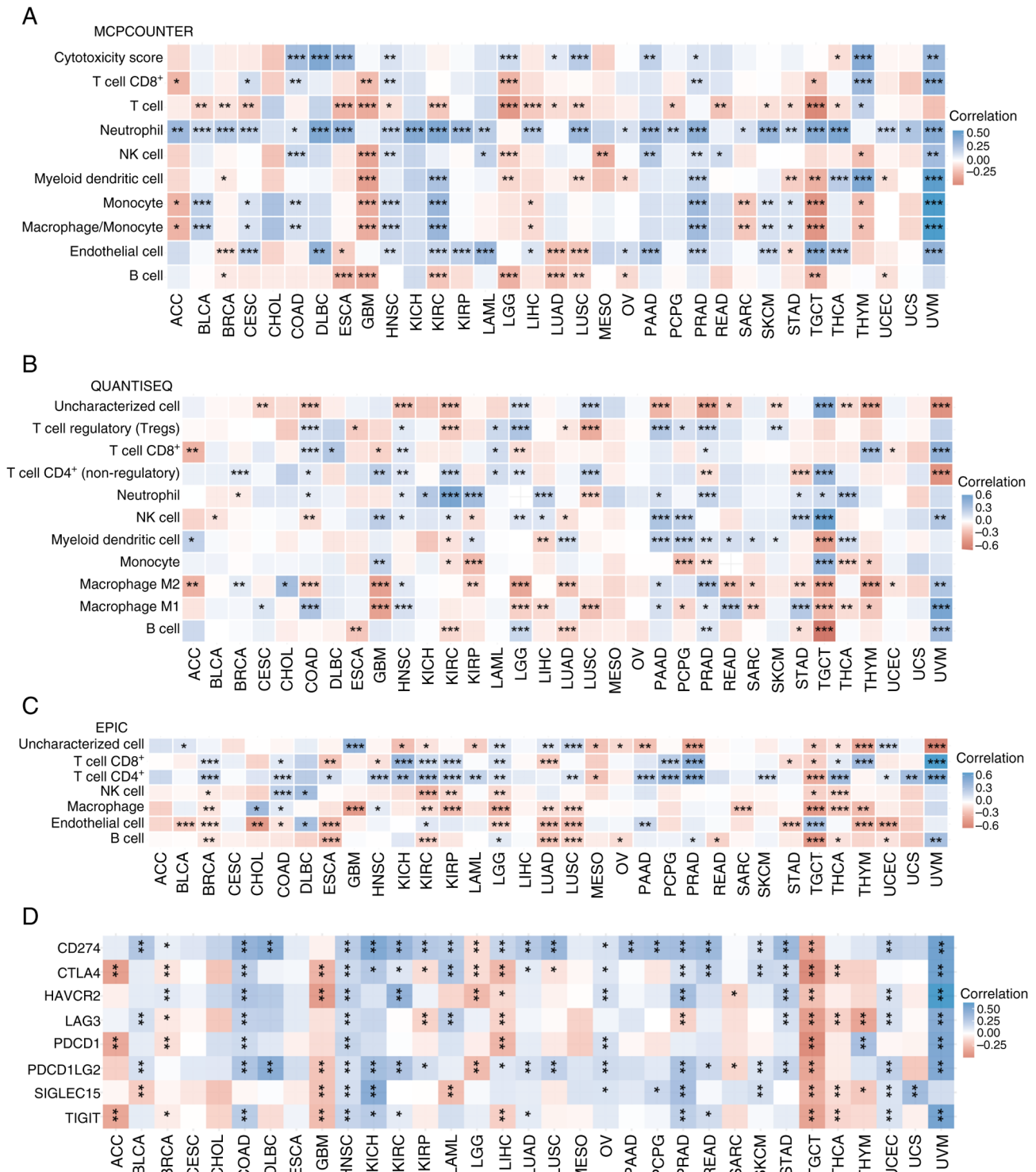


Figure 5. Correlation between SFXN1 and cancer immunity. Correlation between SFXN1 and immune infiltration analyzed by (A) MCPYCOUNTER, (B) QUANTISEQ and (C) EPIC algorithms. (D) Correlation of SFXN1 with immune checkpoint-related gene expression. * $P < 0.05$, ** $P < 0.01$ and *** $P < 0.001$. NK, natural killer; SFXN1, sideroflexin 1.

infiltration in BRCA, COAD, ESCA, HNSC, KICH, KIRC, KIRP, LAML, LGG, LUSC, PAAD, PCPG, PRAD, SKCM, THCA, UCEC, UCS and UVM. EPIC showed a negative association between SFXN1 expression and NK cells in BRCA, KIRC, KIRP, LGG, TGCT and THCA, and a positive association between SFXN1 expression and NK cells in COAD and DLBC. SFXN1 expression exhibited a negative association with macrophage infiltration in BRCA, GBM, KIRC, KIRP,

LGG, LUAD, LUSC, SARC, TGCT, THCA and THYM, but a positive association with macrophage infiltration in CHOL and HNSC. As for the association between SFXN1 expression and endothelial cell infiltration, it showed a negative association in BLCA, BRCA, CHOL, COAD, ESCA, LGG, LUAD, LUSC, STAD, THYM and UCEC, and a positive association in DLBC, KIRC, PAAD and TGCT. SFXN1 expression was negatively associated with B cell infiltration in BRCA, ESCA,

KIRC, LUAD, LUSC, OV, READ, TGCT, THCA and UCEC, but positively associated with B cell infiltration in LGG, PRAD and UVM (Fig. 5C).

To delve deeper into the relationship between SFXN1 and tumor immunity, an analysis of the association between SFXN1 and immune checkpoint molecules in 33 distinct types of cancer tissues was conducted. A negative association between SFXN1 expression and CTLA4, PDCD1 and TIGIT was shown in ACC. In BLCA, SFXN1 expression exhibited a positive correlation with CD274, LAG3 and PDCD1LG2, and a negative correlation with SIGLEC15. In BRCA, SFXN1 expression showed a positive correlation with CD274 and HAVCR2, but a negative correlation with CTLA4, LAG3, PDCD1 and TIGIT. In COAD, a positive association was found between SFXN1 expression and CD274, CTLA4, HAVCR2, LAG3, PDCD1, PDCD1LG2 and TIGIT. A positive correlation was shown in DLBC between SFXN1 expression and CD274 and PDCD1LG2. A negative association between SFXN1 expression and CTLA4, HAVCR2, PDCD1LG2, SIGLEC15 and TIGIT was shown in GBM. In HNSC, SFXN1 expression exhibited a positive correlation with CD274, CTLA4, HAVCR2, LAG3, PDCD1, PDCD1LG2, SIGLEC15 and TIGIT. A positive correlation was shown between SFXN1 expression and CD274, CTLA4, PDCD1LG2, SIGLEC15 and TIGIT in KICH, and between SFXN1 expression and CD274, CTLA4, HAVCR2, PDCD1LG2 and TIGIT in KIRC. However, in KIRP, SFXN1 expression exhibited a positive correlation with CD274 and PDCD1LG2, and a negative correlation with CTLA4 and LAG3. In LAML, a positive association was found between SFXN1 expression and CD274, CTLA4 and LAG3, but a negative correlation with SIGLEC15 was observed. In LGG, a negative correlation was shown between SFXN1 expression and CD274, CTLA4, HAVCR2 and PDCD1LG2. In LIHC, SFXN1 expression exhibited a positive correlation with CD274 and PDCD1LG2, and a negative correlation with CTLA4, HAVCR2, LAG3, PDCD1 and TIGIT. SFXN1 expression exhibited a positive correlation with CD274, CTLA4, PDCD1LG2 and TIGIT in LUAD. In LUSC, a positive association was found between SFXN1 expression and CD274 and PDCD1LG2, while a negative association with CTLA4 was observed. A positive correlation was shown between SFXN1 expression and CD274, CTLA4, HAVCR2, PDCD1, PDCD1LG2 and SIGLEC15 in OV. SFXN1 expression exhibited a positive association with CD274 in PAAD. In PCPG, SFXN1 expression showed a positive correlation with CD274 and SIGLEC15. In PRAD, a positive association was found between SFXN1 expression and CD274, CTLA4, HAVCR2, PDCD1LG2, SIGLEC15 and TIGIT, while a negative association with LAG3 was observed. In READ, SFXN1 expression exhibited a positive correlation with CD274, CTLA4, PDCD1LG2 and TIGIT. A negative association was found between SFXN1 expression and HAVCR2 and PDCD1LG2 in SARC. In SKCM, SFXN1 expression exhibited a positive association with CD274, CTLA4, PDCD1LG2 and SIGLEC15. In STAD, SFXN1 expression showed a positive correlation with CD274, CTLA4, HAVCR2, LAG3 and PDCD1LG2. A negative association was found between SFXN1 expression and CD274, CTLA4, HAVCR2, LAG3, PDCD1, PDCD1LG2, SIGLEC15 and TIGIT in TGCT. In THCA, SFXN1 expression exhibited a negative relationship with CTLA4, LAG3, SIGLEC15 and TIGIT. In THYM, a positive association was found between

SFXN1 expression and PDCD1, whereas a negative association with LAG3 and SIGLEC15 was observed. A positive correlation was shown between SFXN1 expression and CD274, HAVCR2, LAG3, PDCD1LG2, SIGLEC15 and TIGIT in UCEC. In UCS, SFXN1 expression exhibited a positive association with SIGLEC15. SFXN1 expression exhibited a positive correlation with CD274, CTLA4, HAVCR2, LAG3, PDCD1, PDCD1LG2 and TIGIT in UVM. There was no significant correlation between SFXN1 and the expression levels of CD274, CTLA4, HAVCR2, LAG3, PDCD1, PDCD1LG2, SIGLEC15 and TIGIT in CESC, CHOL, ESCA and MESO (Fig. 5D).

A total of six distinct categories were used to classify the immune phenotypes of cancers: C1, wound healing; C2, IFN-dominant; C3, inflammatory; C4, lymphocyte depletion; C5, immunologically quiet; and C6, TGF-dominant. TISIDB was used to explore the relationship between SFXN1 expression and pan-cancer immune subtypes. The findings demonstrated that the immune subtypes of ACC, BLCA, BRCA, COAD, GBM, KIRC, KIRP, LIHC, LUAD, LUSC, OV, PAAD, PRAD, READ, SARC, SKCM, STAD, TGCT, THCA and UCEC were all associated with SFXN1 expression (Fig. S3).

Mutation of SFXN1 in pan-cancer. To probe the mutational landscape of SFXN1 across various cancer types, an extensive search was conducted using cBioPortal. The analysis revealed that KIRC exhibited the highest frequency of SFXN1 alterations, primarily amplifications, which were also observed in SARC, ACC, endometrial cancer, ovarian epithelial tumor, melanoma, NSCLC, pancreatic cancer, bladder cancer, BRCA, prostate cancer, glioma, esophagogastric cancer, renal non-clear cell carcinoma, hepatobiliary cancer and thyroid cancer (Fig. S4A). The overall mutation rate of SFXN1 in pan-cancer was 1.6%. The most prevalent types of SFXN1 mutations in pan-cancer included amplification, deep deletion and missense mutation (Fig. S4B). In addition, a total of 58 genetic alterations were identified in SFXN1, comprising 41 missense, 12 truncating and 5 structural variant/fusion alterations (Fig. S4C).

The relationship between SFXN1 expression and TMB and MSI was also explored. The findings indicated that SFXN1 was positively associated with TMB in COAD ($P<0.001$), HNSC ($P<0.001$), KIRC ($P<0.05$), LUAD ($P<0.001$), PAAD ($P<0.05$), PRAD ($P<0.05$), READ ($P<0.05$), SKCM ($P<0.05$), STAD ($P<0.001$), TGCT ($P<0.05$), THCA ($P<0.001$), UCEC ($P<0.001$) and UCS ($P<0.05$), and negatively correlated with TMB in THYM ($P<0.001$) and UVM ($P<0.05$) (Fig. S4D). SFXN1 was positively associated with MSI in CESC ($P<0.001$), COAD ($P<0.001$), MESO ($P<0.01$), SARC ($P<0.05$), STAD ($P<0.001$), TGCT ($P<0.05$) and UCEC ($P<0.001$) (Fig. S4E).

DNA methylation analysis of SFXN1 in pan-cancer. Utilizing the UALCAN database, a comparative analysis of SFXN1 methylation levels in normal and malignant tissues was conducted. The results indicated that promoter methylation of SFXN1 was significantly increased in BRCA ($P<0.001$), CESC ($P<0.001$), CHOL ($P<0.001$), ESCA ($P<0.01$), HNSC ($P<0.001$), KIRC ($P<0.001$), KIRP ($P<0.001$), LUSC ($P<0.05$), PAAD ($P<0.01$), STAD ($P<0.001$) and SARC ($P<0.001$), whereas it was substantially decreased in PRAD ($P<0.05$), THCA ($P<0.001$) and TGCT ($P<0.001$) (Fig. S5).

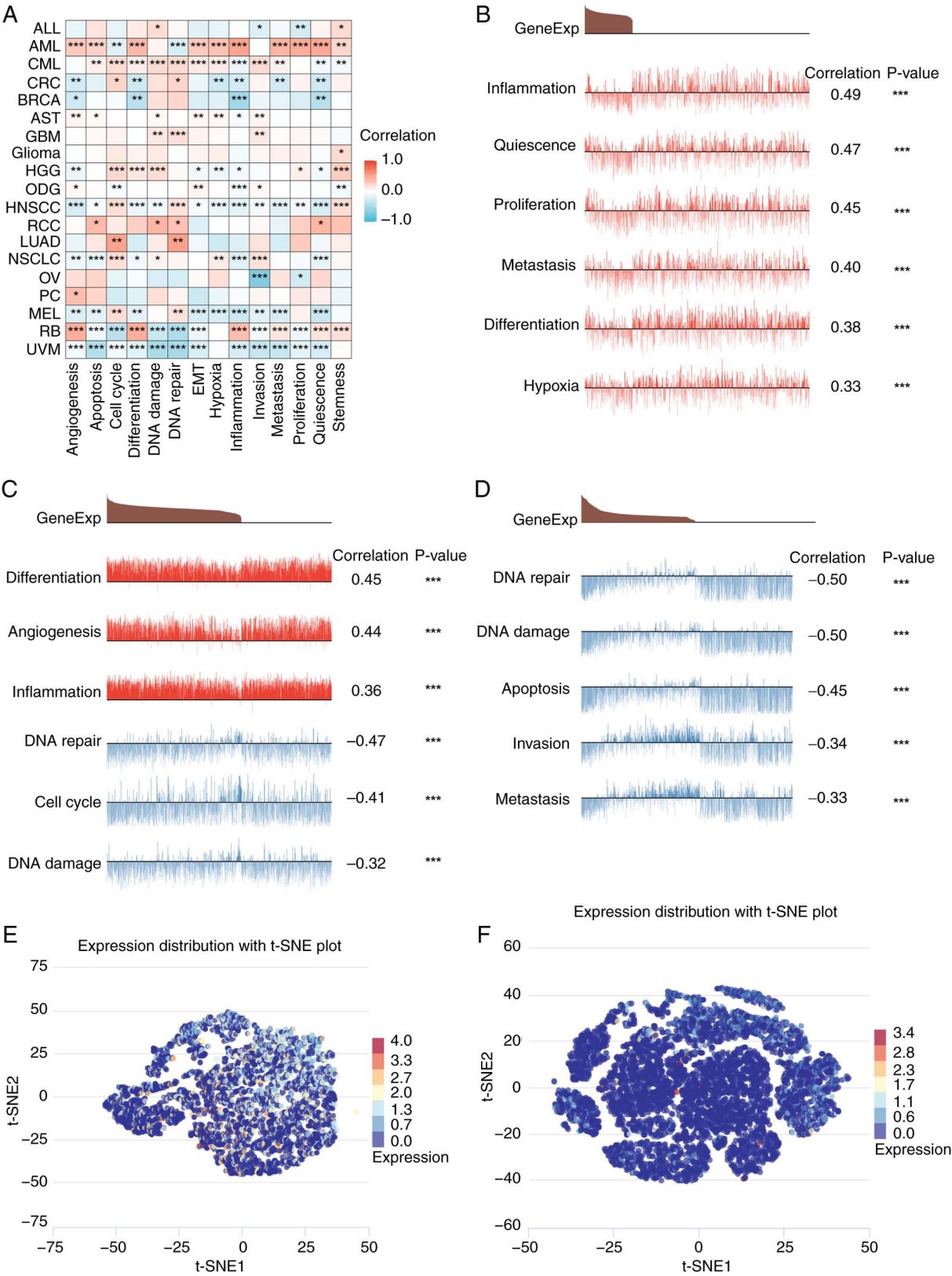


Figure 6. SFXN1 expression at the single-cell level analyzed using CancerSEA. (A) Relationship between SFXN1 expression and different functional states in tumors based on CancerSEA. Correlation between SFXN1 and functional status in (B) AML, (C) RB and (D) UVM. SFXN1 expression profiles in (E) RB and (F) UVM at the single-cell level shown as a t-SNE diagram. * $P < 0.05$, ** $P < 0.01$ and *** $P < 0.001$. EMT, epithelial-mesenchymal transition; SFXN1, sideroflexin 1; t-SNE, t-distributed stochastic neighbor embedding.

SFXN1 expression at the single-cell level. Single-cell sequencing represents a cutting-edge technology enabling the comprehensive analysis of the genome, transcriptome

and epigenome at an unprecedented single-cell resolution. A comparative analysis of the single-cell sequencing data of SFXN1 in pan-cancer was conducted using CancerSEA

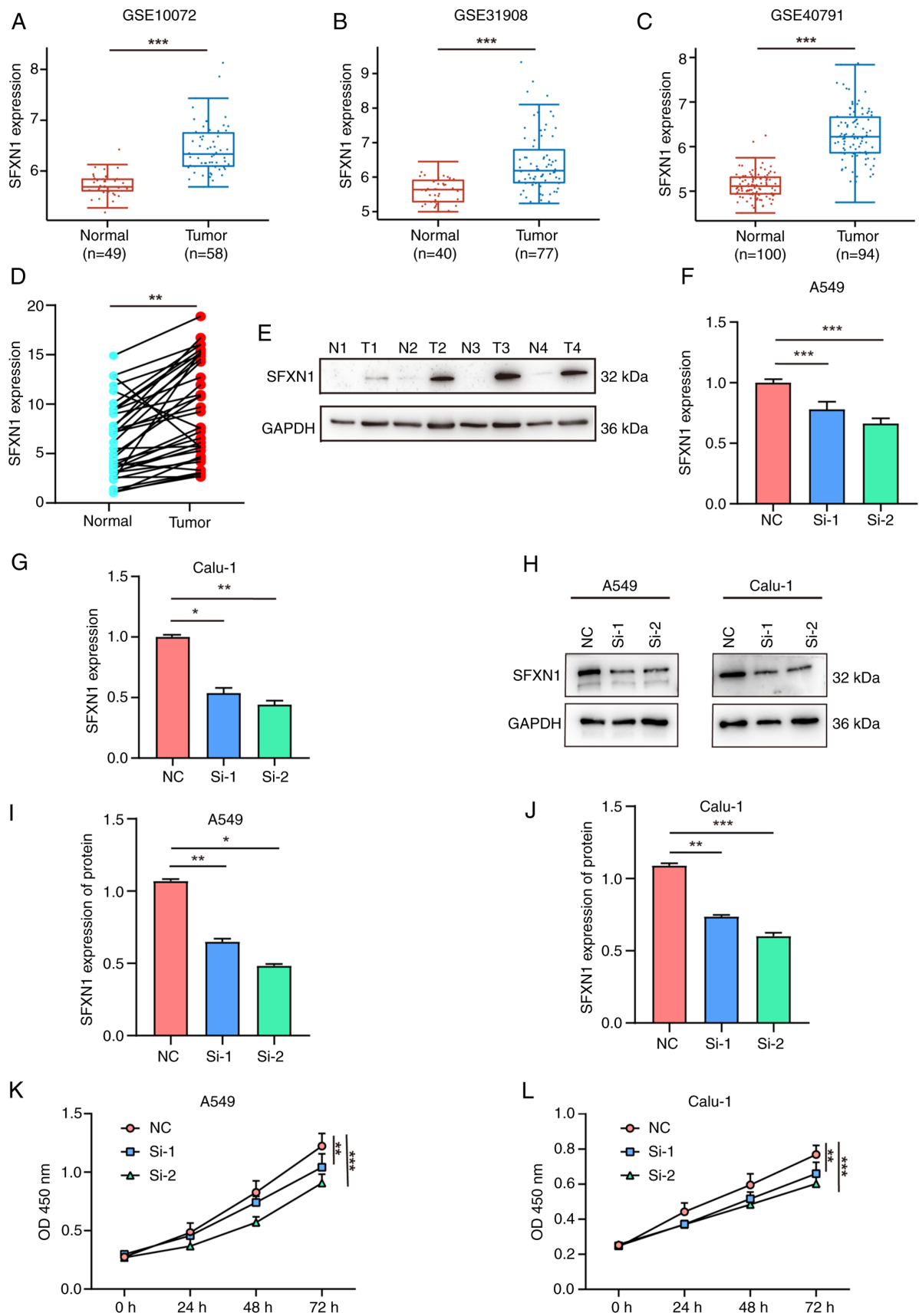


Figure 7. Gene Expression Omnibus validation and cell proliferation assay following SFXN1 knockdown in LUAD cells. External validation of SFXN1 expression in LUAD samples in (A) GSE10072, (B) GSE31908 and (C) GSE40791. (D) Reverse transcription-quantitative PCR and (E) western blot analysis of SFXN1 expression in human LUAD and para-cancerous tissues. (F) Relative mRNA levels of SFXN1 in A549 cells after silencing by siRNAs. (G) Relative mRNA levels of SFXN1 in Calu-1 cells after silencing by siRNAs. (H) Western blot analysis of SFXN1 in A549 and Calu-1 cells at 48 h post-transfection. (I) Relative protein levels of SFXN1 in A549 cells. (J) Relative protein levels of SFXN1 in Calu-1 cells. Cell proliferation following silencing of SFXN1 in (K) A549 and (L) Calu-1 cells was examined using a Cell Counting Kit-8 assay after transfection. * $P < 0.05$, ** $P < 0.01$ and *** $P < 0.001$. LUAD, lung adenocarcinoma; N, normal; T, tumor; OD, optical density; NC, negative control; OD, optical density; SFXN1, sideroflexin 1; siRNA, small interfering RNA; T, tumor.

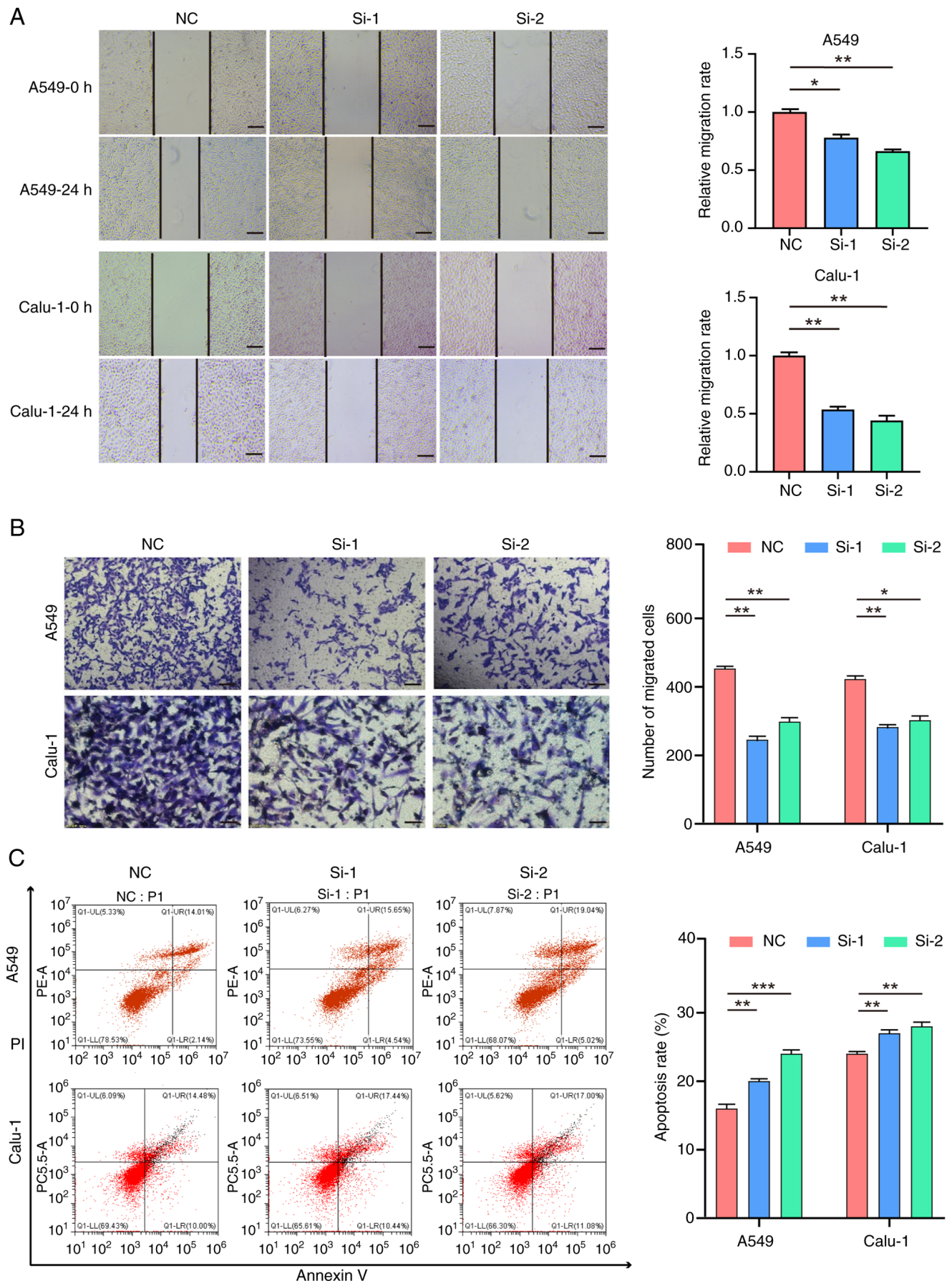


Figure 8. Impaired migration and increased apoptosis following SFXN1 knockdown. (A) A wound healing assay was conducted to determine the migration of transfected A549 and Calu-1 cells. Scale bar, 100 μ m. (B) Transwell assay of transfected A549 and Calu-1 cells. Scale bar, 200 μ m. (C) Increased apoptosis in A549 and Calu-1 cells after SFXN1 knockdown. Data are presented as the mean \pm SD of three independent experiments. * P <0.05, ** P <0.01 and *** P <0.001. NC, negative control; SFXN1, sideroflexin 1; si, small interfering RNA.

(Fig. 6A). In AML, SFXN1 expression was positively correlated with inflammation, quiescence, proliferation, metastasis, differentiation and hypoxia (Fig. 6B). In retinoblastoma (RB), SFXN1 expression was positively correlated with differentiation, angiogenesis and inflammation, and negatively correlated with DNA repair, cell cycle and DNA damage (Fig. 6C). In UVM, SFXN1 expression was negatively correlated with DNA repair, DNA damage, apoptosis, invasion and metastasis (Fig. 6D). In addition, the t-distributed stochastic neighbor embedding maps show the expression profiles of SFXN1 in RB and UVM at the single-cell level (Fig. 6E and F).

SFXN1 expression was analyzed in various normal cells and tissues using the HPA database. Notably, SFXN1 was upregulated in T cells in the bone marrow, lungs, lymph nodes, peripheral blood mononuclear cells, skin and stomach at the single-cell level (Fig. S6).

Related genes of SFXN1 in pan-cancer. The top 200 genes co-expressed with SFXN1 in pan-cancer were extracted from GEPIA2.0 (Table SII). The PPI network was visualized using Cytoscape, and the top 20 genes were identified based on their degree values (Fig. S7). Ultimately, a heatmap was employed to illustrate the positive correlation between SFXN1 and the top 20 genes in pan-cancer (Fig. S8).

Enrichment analysis of SFXN1 in LUAD. Preliminary analysis indicated that SFXN1 could serve as a potential biomarker for both diagnosis and prognosis in a variety of tumor types, with significant dysregulation observed particularly in LUAD. Consequently, an in-depth exploration of the role of SFXN1 in LUAD was conducted. Subsequently, the co-expression genes associated with SFXN1 in LUAD were explored (Table SIII). The top 50 genes positively and negatively correlated with SFXN1 were displayed as heatmaps (Fig. S9A and B). The GO analysis of SFXN1 co-expression genes showed that the main physiological functions involved were 'cell division', 'negative regulation of transcription, DNA-templated' and 'intracellular signal transduction'. The genes related to SFXN1 were mainly located in the 'nucleus', 'cytosol', 'nucleoplasm' and 'membrane', and they mainly had molecular functions such as 'protein binding', 'ATP binding', 'protein kinase binding' and 'chromatin binding' (Fig. S9C-E). The KEGG pathway analysis revealed that SFXN1-related genes were mainly involved in the 'cell cycle', 'oocyte meiosis', 'glycolysis/gluconeogenesis' and 'p53 signaling pathway' (Fig. S9F).

The differentially expressed genes were analyzed by GSEA to explore the possible pathways in which SFXN1 may participate in LUAD. The KEGG pathways identified included 'cell cycle', 'PLK1 pathway', 'cell cycle checkpoints', 'FOXM1 pathway', 'G2 M checkpoints', 'G1 S specific transcription', 'mitotic spindle checkpoint', 'DNA strand elongation' and 'DNA replication' (Fig. S10).

GEO validation and the oncogenic role of SFXN1 in LUAD. To confirm the mRNA expression levels of SFXN1 in patients with LUAD, GEO was searched and a marked increase in SFXN1 expression was observed in the GSE10072 (42), GSE31908 (43) and GSE40791 (44) datasets (Fig. 7A-C).

Furthermore, 35 pairs of LUAD and adjacent non-cancerous tissues were collected to detect SFXN1 expression. The results showed that SFXN1 mRNA expression was markedly upregulated in LUAD tissues compared with normal tissues ($P < 0.01$; Fig. 7D). Additionally, the protein levels of SFXN1 in LUAD tissues were found to be higher than those in the adjacent non-cancerous tissues (Fig. 7E).

siRNAs were utilized to knock down SFXN1 expression in lung cancer cell lines, and the transfection efficiency was verified by RT-qPCR and western blotting. siRNA transfection notably reduced SFXN1 expression at both the mRNA (Fig. 7F and G) and protein levels (Fig. 7H-J). Additionally, the CCK-8 cell proliferation assay demonstrated that SFXN1 knockdown could significantly inhibit the proliferation of A549 and Calu-1 cells (Fig. 7K and L).

The scratch wound healing assay revealed that the scratch widths at 48 h of the si-1 and si-2 groups were larger than those of the control (NC) group, indicating that the knockdown of SFXN1 diminished the wound healing capacity of A549 and Calu-1 cells (Fig. 8A). Additionally, the Transwell assay demonstrated that silencing of SFXN1 expression curtailed the invasion of A549 and Calu-1 cells (Fig. 8B). Finally, flow cytometry was employed to assess cell apoptosis, and the findings indicated that knockdown of SFXN1 expression enhanced the apoptotic rate of A549 and Calu-1 cells (Fig. 8C).

Discussion

With the rapid advancement of immunotherapy and targeted therapy, there is an urgent need to identify novel cancer biomarkers and explore innovative treatments strategies. SFXN1, a member of the SFXN family, is a mitochondrial protein inserted into the inner mitochondrial membrane. Despite its known biological significance, the molecular functions of SFXN1 remain largely elusive (45). It has been reported that SFXN1 functions as a serine transporter in one-carbon metabolism (11). The role of SFXN1 in transporting pyridoxine (vitamin B6) within the mitochondria is supported by evidence that animals lacking SFXN1 exhibit phenotypes resembling those of human disorders such as X-linked iron granulocyte anemia, which are associated with pyridoxine deficiency or ALAS2 mutations (46). In addition, SFXN1 has been implicated in conditions such as osteoarthritis and heart hypertrophy (47,48). Ferroptosis, a form of programmed cell death, is dependent on iron and driven by lipid peroxidation, marked by the accumulation of ROS and lipid peroxides (49). SFXN1 is involved in lipopoly-saccharide-induced ferroptosis in H9C2 cardiomyocytes, although the underlying molecular mechanisms remain to be elucidated (15). Emerging research has indicated that SFXN1 contributes to the initiation, progression and prognosis of BRCA (50), LUAD (51) and non-viral LIHC (14). Therefore, to gain a deeper understanding of the role of SFXN1 in tumorigenesis and its potential regulatory pathways, bioinformatics tools such as TCGA, UALCAN and cBioPortal were employed to reveal the gene expression pattern, prognostic implications, gene mutation and DNA methylation of SFXN1 in 33 tumor types.

The tumor microenvironment (TME) encompasses the complex milieu in which the tumor, invasive immune cells and

stromal cells coexist and interact. Research has underscored the pivotal role of immune cell infiltration in tumor progression and response to immunotherapy (52). The present findings indicated that SFXN1 expression was associated with the infiltration of CD4⁺ T and CD8⁺ T cells. Furthermore, high SFXN1 expression in T cells at the single-cell level indicated that SFXN1 may serve a role in T cell immune responses. Additionally, the observed positive and negative correlation between SFXN1 expression and the expression of immune checkpoints implied that SFXN1 could represent a promising target for the development of cancer immunotherapies. These insights highlight the potential of SFXN1 as a biomarker and therapeutic target, warranting further investigation into its mechanistic role in modulating the TME and immune response to tumors.

Previous studies have indicated that tumors with elevated TMB and MSI scores tend to respond more favorably to immunotherapy (53,54). The present investigation of the relationship between SFXN1 expression and both TMB and MSI demonstrated a positive correlation between SFXN1 expression and TMB and MSI scores in several tumor types. Consequently, we hypothesized that the heightened SFXN1 expression in malignancies might confer post-immunotherapy survival advantages to patients. Given these findings, SFXN1 could emerge as a potential novel therapeutic target for immunotherapy in the treatment of various cancer types.

DNA methylation, one of the most prevalent epigenetic modifications, serves a crucial role in carcinogenesis, genomic stability and gene expression regulation. It has been reported that abnormal DNA methylation can accelerate tumor growth by modulating cell proliferation, apoptosis and senescence (55). The present analysis using UALCAN revealed elevated levels of SFXN1 promoter methylation in certain tumor types, including BRCA, CESC, CHOL, ESCA, HNSC, KIRC, KIRP, LUSC, PAAD, STAD and SARC. By contrast, a pronounced reduction in SFXN1 promoter methylation was observed in PRAD, THCA and TGCT. These findings suggest that the differential methylation status of the SFXN1 promoter may exert distinct effects on tumor biology, potentially influencing the progression and behavior of various cancer types.

The present study identified that SFXN1 was highly expressed in LUAD and was associated with poor prognosis, which was one of the primary reasons for the focus on this particular cancer type. Additionally, our research team has been dedicated to lung cancer research for several years, bringing a wealth of expertise and a deep understanding of the field to bear on this investigation. The broader implications of SFXN1 in other cancer types and the need for further research are acknowledged. The present study lays the groundwork for future exploration of the role of SFXN1 in LUAD and potentially other tumor types. However, notwithstanding these findings, the present study has certain limitations. Analyses and verifications were performed using databases and fundamental cellular experiments, but the present study lacks a more profound investigation of the underlying molecular mechanisms, an aspect that should be addressed in future studies. The confirmation through external datasets and the examination of freshly collected paired tissues lend credibility and reliability to the present results. These findings offer a novel perspective for investigating the mechanisms of tumorigenesis, progression and therapeutic response.

In conclusion, the present comprehensive pan-cancer analysis of SFXN1 demonstrated its differential expression across several cancer types and its significant association with OS and DFS in patients with KIRC and MESO. These findings underscore the potential of SFXN1 as a prognostic biomarker, offering valuable insights for the identification of novel tumor-related therapeutic targets. The present study not only enhances the understanding of the role of SFXN1 in cancer but also paves the way for future investigations aimed at harnessing its predictive capabilities for improved patient outcomes.

Acknowledgements

Not applicable.

Funding

The present study was supported by the National Natural Science Foundation of China (grant nos. 81800182 and 81802290).

Availability of data and materials

The data generated in the present study may be requested from the corresponding author.

Authors' contributions

LZ, SW and LW designed and performed bioinformatics analysis. LZ conducted cell experiments, analyzed the data and organized the images. LZ and LW wrote and revised the paper. LZ and LW confirm the authenticity of all the raw data. All authors read and approved the final version of the manuscript.

Ethics approval and consent to participate

Written informed consent was obtained from all participants prior to the study. The Ethics Committee of the Affiliated Hospital of Jining Medical University (Jining, China) evaluated and approved this work (approval no. 2021-11-C009) in accordance with the principles of The Declaration of Helsinki.

Patient consent for publication

Not applicable.

Competing interests

The authors declare that they have no competing interests.

References

1. Sung H, Ferlay J, Siegel RL, Laversanne M, Soerjomataram I, Jemal A and Bray F: Global cancer statistics 2020: GLOBOCAN estimates of incidence and mortality worldwide for 36 cancers in 185 countries. *CA Cancer J Clin* 71: 209-249, 2021.
2. Rajurkar S, Mambetsariev I, Pharaon R, Leach B, Tan T, Kulkarni P and Salgia R: Non-small cell lung cancer from genomics to therapeutics: A framework for community practice integration to arrive at personalized therapy strategies. *J Clin Med* 9: 1870, 2020.

3. Tifoun N, De Las Heras JM, Guillaume A, Bouleau S, Mignotte B and Le Floch N: Insights into the roles of the sideroflexins/SLC56 family in iron homeostasis and iron-sulfur biogenesis. *Biomedicines* 9: 103, 2021.
4. Miotto G, Tessaro S, Rotta GA and Bonatto D: In silico analyses of Fsf1 sequences, a new group of fungal proteins orthologous to the metazoan sideroblastic anemia-related sideroflexin family. *Fungal Genet Biol* 44: 740-753, 2007.
5. Burgos-Barragan G, Wit N, Meiser J, Dingler FA, Pietzke M, Mulderrig L, Pontel LB, Rosado IV, Brewer TF, Cordell RL, *et al*: Mammals divert endogenous genotoxic formaldehyde into one-carbon metabolism. *Nature* 548: 549-554, 2017.
6. Ducker GS and Rabinowitz JD: One-carbon metabolism in health and disease. *Cell Metab* 25: 27-42, 2017.
7. Fu TF, Rife JP and Schirch V: The role of serine hydroxymethyltransferase isozymes in one-carbon metabolism in MCF-7 cells as determined by (13)C NMR. *Arch Biochem Biophys* 393: 42-50, 2001.
8. Rivell A, Petralia RS, Wang YX, Mattson MP and Yao PJ: Sideroflexin 3 is a mitochondrial protein enriched in neurons. *Neuromolecular Med* 21: 314-321, 2019.
9. Mon EE, Wei FY, Ahmad RNR, Yamamoto T, Moroishi T and Tomizawa K: Regulation of mitochondrial iron homeostasis by sideroflexin 2. *J Physiol Sci* 69: 359-373, 2019.
10. Fleming MD, Campagna DR, Haslett JN, Trenor CC III and Andrews NC: A mutation in a mitochondrial transmembrane protein is responsible for the pleiotropic hematological and skeletal phenotype of flexed-tail (f/f) mice. *Genes Dev* 15: 652-657, 2001.
11. Kory N, Wyant GA, Prakash G, Uit de Bos J, Bottanelli F, Pacold ME, Chan SH, Lewis CA, Wang T, Keys HR, *et al*: SFXN1 is a mitochondrial serine transporter required for one-carbon metabolism. *Science* 362: eaat9528, 2018.
12. Weston C, Klobusicky J, Weston J, Connor J, Toms SA and Marko NF: Aberrations in the iron regulatory gene signature are associated with decreased survival in diffuse infiltrating gliomas. *PLoS One* 11: e0166593, 2016.
13. Chen Q, Wang R, Zhang J and Zhou L: Sideroflexin1 as a novel tumor marker independently predicts survival in lung adenocarcinoma. *Transl Cancer Res* 8: 1170-1178, 2019.
14. Yagi K, Shimada S, Akiyama Y, Hatano M, Asano D, Ishikawa Y, Ueda H, Watanabe S, Akahoshi K, Ono H, *et al*: Loss of SFXN1 mitigates lipotoxicity and predicts poor outcome in non-viral hepatocellular carcinoma. *Sci Rep* 13: 9449, 2023.
15. Li N, Wang W, Zhou H, Wu Q, Duan M, Liu C, Wu H, Deng W, Shen D and Tang Q: Ferritinophagy-mediated ferroptosis is involved in sepsis-induced cardiac injury. *Free Radic Biol Med* 160: 303-318, 2020.
16. Navani S: Manual evaluation of tissue microarrays in a high-throughput research project: The contribution of Indian surgical pathology to the human protein atlas (HPA) project. *Proteomics* 16: 1266-1270, 2016.
17. Tomczak K, Czerwińska P and Wiznerowicz M: The cancer genome atlas (TCGA): An immeasurable source of knowledge. *Contemp Oncol (Pozn)* 19: A68-A77, 2015.
18. Li T, Fan J, Wang B, Traugh N, Chen Q, Liu JS, Li B and Liu XS: TIMER: A web server for comprehensive analysis of tumor-infiltrating immune cells. *Cancer Res* 77: e108-e110, 2017.
19. Liu RZ, Graham K, Glubrecht DD, Germain DR, Mackey JR and Godbout R: Association of FABP5 expression with poor survival in triple-negative breast cancer: Implication for retinoic acid therapy. *Am J Pathol* 178: 997-1008, 2011.
20. Ryan BM, Zanetti KA, Robles AI, Schetter AJ, Goodman J, Hayes RB, Huang WY, Gunter MJ, Yeager M, Burdette L, *et al*: Germline variation in NCF4, an innate immunity gene, is associated with an increased risk of colorectal cancer. *Int J Cancer* 134: 1399-1407, 2014.
21. Nicolau-Neto P, Da Costa NM, de Souza Santos PT, Gonzaga IM, Ferreira MA, Guaraldi S, Moreira MA, Seuánez HN, Brewer L, Bergmann A, *et al*: Esophageal squamous cell carcinoma transcriptome reveals the effect of FOXM1 on patient outcome through novel PIK3R3 mediated activation of PI3K signaling pathway. *Oncotarget* 9: 16634-16647, 2018.
22. Verduci L, Ferraiuolo M, Sacconi A, Ganci F, Vitale J, Colombo T, Paci P, Strano S, Macino G, Rajewsky N and Blandino G: The oncogenic role of circPVT1 in head and neck squamous cell carcinoma is mediated through the mutant p53/YAP/TEAD transcription-competent complex. *Genome Biol* 18: 237, 2017.
23. Nazarov PV, Muller A, Kaoma T, Nicot N, Maximo C, Birembaut P, Tran NL, Dittmar G and Vallar L: RNA sequencing and transcriptome arrays analyses show opposing results for alternative splicing in patient derived samples. *BMC Genomics* 18: 443, 2017.
24. Selamat SA, Chung BS, Girard L, Zhang W, Zhang Y, Campan M, Siegmund KD, Koss MN, Hagen JA, Lam WL, *et al*: Genome-scale analysis of DNA methylation in lung adenocarcinoma and integration with mRNA expression. *Genome Res* 22: 1197-1211, 2012.
25. Pei H, Li L, Fridley BL, Jenkins GD, Kalari KR, Lingle W, Petersen G, Lou Z and Wang L: FKBP51 affects cancer cell response to chemotherapy by negatively regulating Akt. *Cancer Cell* 16: 259-266, 2009.
26. Cui J, Chen Y, Chou WC, Sun L, Chen L, Suo J, Ni Z, Zhang M, Kong X, Hoffman LL, *et al*: An integrated transcriptomic and computational analysis for biomarker identification in gastric cancer. *Nucleic Acids Res* 39: 1197-1207, 2011.
27. Chandrashekar DS, Karthikeyan SK, Korla PK, Patel H, Shovon AR, Athar M, Netto GJ, Qin ZS, Kumar S, Manne U, *et al*: UALCAN: An update to the integrated cancer data analysis platform. *Neoplasia* 25: 18-27, 2022.
28. Chandrashekar DS, Bashel B, Balasubramanya SAH, Creighton CJ, Ponce-Rodriguez I, Chakravarthi BVSK and Varambally S: UALCAN: A portal for facilitating tumor subgroup gene expression and survival analyses. *Neoplasia* 19: 649-658, 2017.
29. Lánckzy A and Györfy B: Web-based survival analysis tool tailored for medical research (KMplot): Development and implementation. *J Med Internet Res* 23: e27633, 2021.
30. Tang Z, Li C, Kang B, Gao G, Li C and Zhang Z: GEPIA: A web server for cancer and normal gene expression profiling and interactive analyses. *Nucleic Acids Res* 45 (W1): W98-W102, 2017.
31. Gao J, Aksoy BA, Dogrusoz U, Dresdner G, Gross B, Sumer SO, Sun Y, Jacobsen A, Sinha R, Larsson E, *et al*: Integrative analysis of complex cancer genomics and clinical profiles using the cBioPortal. *Sci Signal* 6: pii, 2013.
32. Cao J, Yang X, Chen S, Wang J, Fan X, Fu S and Yang L: The predictive efficacy of tumor mutation burden in immunotherapy across multiple cancer types: A meta-analysis and bioinformatics analysis. *Transl Oncol* 20: 101375, 2022.
33. Fumet JD, Truntzer C, Yarchoan M and Ghiringhelli F: Tumour mutational burden as a biomarker for immunotherapy: Current data and emerging concepts. *Eur J Cancer* 131: 40-50, 2020.
34. Ansari A, Ray SK, Sharma M, Rawal R and Singh P: Tumor mutational burden as a biomarker of immunotherapy response: An immunogram approach in onco-immunology. *Curr Mol Med* 24: 1461-1469, 2024.
35. Strickler JH, Hanks BA and Khasraw M: Tumor mutational burden as a predictor of immunotherapy response: Is more always better? *Clin Cancer Res* 27: 1236-1241, 2021.
36. Steuer CE and Ramalingam SS: Tumor mutation burden: Leading immunotherapy to the era of precision medicine? *J Clin Oncol* 36: 631-632, 2018.
37. Yang G, Zheng RY and Jin ZS: Correlations between microsatellite instability and the biological behaviour of tumours. *J Cancer Res Clin Oncol* 145: 2891-2899, 2019.
38. Yuan H, Yan M, Zhang G, Liu W, Deng C, Liao G, Xu L, Luo T, Yan H, Long Z, *et al*: CancerSEA: A cancer single-cell state atlas. *Nucleic Acids Res* 47 (D1): D900-D908, 2019.
39. Huang da W, Sherman BT and Lempicki RA: Systematic and integrative analysis of large gene lists using DAVID bioinformatics resources. *Nat Protoc* 4: 44-57, 2009.
40. Schag CC, Heinrich RL and Ganz PA: Karnofsky performance status revisited: Reliability, validity, and guidelines. *J Clin Oncol* 2: 187-193, 1984.
41. Livak KJ and Schmittgen TD: Analysis of relative gene expression data using real-time quantitative PCR and the 2(-Delta Delta C(T)) method. *Methods* 25: 402-408, 2001.
42. Landi MT, Dracheva T, Rotunno M, Figueroa JD, Liu H, Dasgupta A, Mann FE, Fukuoka J, Hames M, Bergen AW, *et al*: Gene expression signature of cigarette smoking and its role in lung adenocarcinoma development and survival. *PLoS One* 3: e1651, 2008.
43. Wu J, Zhou L, Huang L, Gu J, Li S, Liu B, Feng J and Zhou Y: Nomogram integrating gene expression signatures with clinicopathological features to predict survival in operable NSCLC: A pooled analysis of 2164 patients. *J Exp Clin Cancer Res* 36: 4, 2017.

44. Zhang Y, Foreman O, Wigle DA, Kosari F, Vasmatazis G, Salisbury JL, van Deursen J and Galaray PJ: USP44 regulates centrosome positioning to prevent aneuploidy and suppress tumorigenesis. *J Clin Invest* 122: 4362-4374, 2012.
45. Acoba MG, Alpergin ESS, Renuse S, Fernández-Del-Río L, Lu YW, Khalimonchuk O, Clarke CF, Pandey A, Wolfgang MJ and Claypool SM: The mitochondrial carrier SFXN1 is critical for complex III integrity and cellular metabolism. *Cell Rep* 34: 108869, 2021.
46. Ye X, Xu J, Cheng C, Yin G, Zeng L, Ji C, Gu S, Xie Y and Mao Y: Isolation and characterization of a novel human putative anemia-related gene homologous to mouse sideroflexin. *Biochem Genet* 41: 119-125, 2003.
47. Tang M, Huang Z, Luo X, Liu M, Wang L, Qi Z, Huang S, Zhong J, Chen JX, Li L, *et al*: Ferritinophagy activation and sideroflexin1-dependent mitochondria iron overload is involved in apelin-13-induced cardiomyocytes hypertrophy. *Free Radic Biol Med* 134: 445-457, 2019.
48. Huang H, Zheng J, Shen N, Wang G, Zhou G, Fang Y, Lin J and Zhao J: Identification of pathways and genes associated with synovitis in osteoarthritis using bioinformatics analyses. *Sci Rep* 8: 10050, 2018.
49. Dixon SJ, Lemberg KM, Lamprecht MR, Skouta R, Zaitsev EM, Gleason CE, Patel DN, Bauer AJ, Cantley AM, Yang WS, *et al*: Ferroptosis: an iron-dependent form of nonapoptotic cell death. *Cell* 149: 1060-1072, 2012.
50. Andriani L, Ling YX, Yang SY, Zhao Q, Ma XY, Huang MY, Zhang YL, Zhang FL, Li DQ and Shao ZM: Sideroflexin-1 promotes progression and sensitivity to lapatinib in triple-negative breast cancer by inhibiting TOLLIP-mediated autophagic degradation of CIP2A. *Cancer Lett* 597: 217008, 2024.
51. Li Y, Yang W, Liu C, Zhou S, Liu X, Zhang T, Wu L, Li X, Zhang J and Chang E: SFXN1-mediated immune cell infiltration and tumorigenesis in lung adenocarcinoma: A potential therapeutic target. *Int Immunopharmacol* 132: 111918, 2024.
52. Sadeghi Rad H, Monkman J, Warkiani ME, Ladwa R, O'Byrne K, Rezaei N and Kulasinghe A: Understanding the tumor micro-environment for effective immunotherapy. *Med Res Rev* 41: 1474-1498, 2021.
53. Filipovic A, Miller G and Bolen J: Progress toward identifying exact proxies for predicting response to immunotherapies. *Front Cell Dev Biol* 8: 155, 2020.
54. Reck M, Schenker M, Lee KH, Provencio M, Nishio M, Lesniewski-Kmak K, Sangha R, Ahmed S, Raimbourg J, Feeney K, *et al*: Nivolumab plus ipilimumab versus chemotherapy as first-line treatment in advanced non-small-cell lung cancer with high tumour mutational burden: Patient-reported outcomes results from the randomised, open-label, phase III CheckMate 227 trial. *Eur J Cancer* 116: 137-147, 2019.
55. Pfeifer GP: Defining driver DNA methylation changes in human cancer. *Int J Mol Sci* 19: 1166, 2018.



Copyright © 2025 Zhang et al. This work is licensed under a Creative Commons Attribution-NonCommercial-NoDerivatives 4.0 International (CC BY-NC-ND 4.0) License.